UDC 517.9

MODELLING THE PHASE SYNCHRONIZATION IN SYSTEMS OF TWO AND THREE COUPLED OSCILLATORS

МОДЕЛЮВАННЯ ФАЗОВОЇ СИНХРОНІЗАЦІЇ В СИСТЕМАХ ДВОХ І ТРЬОХ ЗВ'ЯЗАНИХ ОСЦИЛЯТОРІВ

A. Vasylenko

Inst. Math. Nat. Acad. Sci. Ukraine
Ukraine, 01601, Kyiv 4, Tereshchenkivska Str., 3
e-mail: Ann@imath.kiev.ua

Yu. Maistrenko

Inst. Math. Nat. Acad. Sci. Ukraine
Ukraine, 01601, Kyiv 4, Tereshchenkivska Str., 3

M. Hasler

Swiss Federal Institute Technol.
CH-1015, Lausanne, Switzerland

We obtain regions of synchronization of two and three globally coupled oscillators, and describe the main mechanisms and bifurcations through which the systems synchronization is lost.

Отримано області синхронізації двох та трьох глобально зв'язаних осциляторів. Описано основні механізми та біфуркації, через які втрачається синхронізація в розглянутих системах.

1. Introduction. Phase synchronization is one of the fundamental and universal nonlinear phenomena in physics, engineering, biology, economics and other fields of science and technology [1 – 4]. Synchronization occurs if some oscillatory systems interact and adjust their behaviours to one another in order to achieve a state where they oscillate in unison, the state of synchronization. Well-known examples of the synchronization are the example of two clocks or pendulums hanging on a wall which come to the synchronized state due to the interaction through the wall, the synchronization of the rotation of the moon with its orbital motion, so that the moon always shows the same side towards the earth.

In the present paper we investigate the phase synchronization of two and three globally coupled nonlinear oscillators (or clocks) whose individual dynamics are described by the shift circle maps. Ensembles of the coupled oscillators model a wide variety of different phenomena. Investigation of their dynamics is particularly of interest in connection with different engineering and communication problems, for example transmitting information [5].

The paper is organized as follows. In Section 2 first we introduce the two-dimensional discrete-time system of the globally coupled circle maps coupled with the sine-coupling, and briefly describe the dynamics of analogue continuous-time model emphasizing some differences and common features of these two systems. Then we describe the dynamics of the discrete-time system of the coupled oscillators. We outline the regions of the phase synchronization and explain the bifurcations through which the synchronization is lost. In Section 3 we carry out a

similar analysis for three globally coupled circle maps, starting from several particular cases and coming to their generalization. In particular we outline the synchronization regions for three identical oscillators and then for the system of two identical oscillators and the third one being different from them. For this latter case we also investigate in detail how the system equilibria change with varying the parameter values. The paper ends with the section of conclusions.

2. Synchronization in the system of two coupled oscillators. ***2.1. The model.*** Let us consider the system of two coupled oscillators or clocks whose dynamics are described by the Arnold circle maps

$$\begin{aligned} x_{n+1} &= x_n + 2\pi\nu_1 + \frac{K}{2}\sin(y_n - x_n), \\ y_{n+1} &= y_n + 2\pi\nu_2 + \frac{K}{2}\sin(x_n - y_n), \end{aligned} \tag{1}$$

where both the variables x and y are calculated modulo 2π. System (1) describes the dynamics of two phase oscillators with the corresponding frequencies ν_1 and ν_2, which are mutually coupled with the sine coupling and K is the coupling strength.

The synchronization of the oscillators can be expressed in terms of the difference between the phase variables x_n and y_n. After subtracting the second equation of the system from the first one the following equation for the phase difference is obtained:

$$x_{n+1} - y_{n+1} = x_n - y_n + 2\pi(\nu_1 - \nu_2) - K\sin(x_n - y_n)$$

or after introducing the new variable $z_n = x_n - y_n$,

$$z_{n+1} = z_n + 2\pi(\nu_1 - \nu_2) - K\sin z_n, \tag{2}$$

where z is calculated modulo 2π. Therefore we can conclude that the dynamics of the phase difference are described by the well known sine circle map, and the synchronization for the system (1) can be achieved, e.g. with the parameter values for which the map (2) has an attracting fixed point.

2.2. Continuous-time Kuramoto system. It is worth emphasizing that the system (1) is a discrete analog of a so called Kuramoto system [6],

$$\dot{\psi}_i = \omega_i + \frac{K}{N}\sum_{j=1}^{N}\sin(\psi_j - \psi_i). \tag{3}$$

The simplest example $N = 2$,

$$\begin{aligned} \dot{\psi}_1 &= \omega_1 + \frac{K}{2}\sin(\psi_2 - \psi_1), \\ \dot{\psi}_2 &= \omega_2 + \frac{K}{2}\sin(\psi_1 - \psi_2), \end{aligned} \tag{4}$$

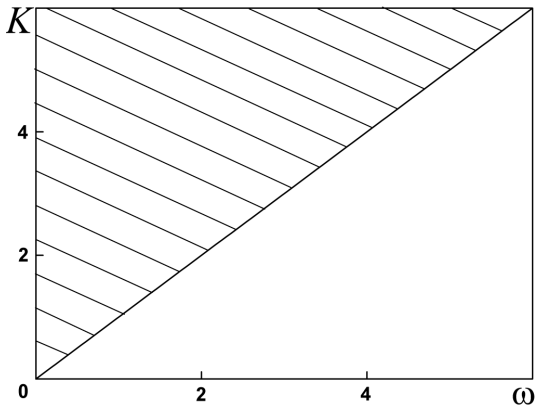

Fig. 1. Stability diagram for the equation (5). For the parameter values from the shaded region a stable equilibrium exists, and therefore the Kuramoto system (4) is synchronized.

where $0 \leq \psi_i \leq 2\pi$. If we consider the difference between the equations of this system, then we obtain the following differential equation:

$$\dot{\varphi} = \omega - K \sin \varphi, \tag{5}$$

where $\varphi = \psi_1 - \psi_2$ is the difference of the phase variables and $\omega = \omega_1 - \omega_2$ the difference of the angular frequencies. The fixed point $\varphi^* = \arcsin\dfrac{\omega}{K}$ corresponds to the constant phase difference $\psi_1 - \psi_2$ and therefore is a state of synchronization. This fixed point exists and is stable for the values of ω and K such that $\left|\dfrac{\omega}{K}\right| \leq 1$, as shown in Fig. 1, and there are no other periodic orbits for this equation.

2.3. Synchronization regions for the discrete-time model. An analysis of the dynamics of the discrete Kuramoto model (1) can be performed following the ideology of the paper [7]. The Arnol'd sine circle map (2) describes the dynamics of the phase difference for our system of coupled oscillators, and depending on the parameter values this map exhibits periodic or quasiperiodic behaviour. While considering two identical oscillators in (1), i. e., $\nu_1 = \nu_2$, the map (2) has the fixed point $z^* = 0$ which corresponds to the full synchronization in (1), $|x_n - y_n| \to 0$ as $n \to \infty$. For the oscillators with different frequencies ν_1 and ν_2 the fixed point is $z^* = \arcsin\dfrac{2\pi\,(\nu_1 - \nu_2)}{K}$, and its stability, if it takes place, means that the oscillators are synchronized but with a nonzero phase difference $|x_n - y_n| \to z^*$ as $n \to \infty$. Unlike the case of the continuous-time Kuramoto system, the map (2) can also exhibit synchronized periodic orbits of higher periods as well as synchronized chaotic motion, when there exist $C > 0$: $|z_n| < C \ \ \forall n$. Coming back to the variables x_n and y_n, existence and stability of the q-periodic orbit of the map (2) means that the oscillators are synchronized so that their phase difference $z_n = x_n - y_n$ changes between q constant values. Therefore we have 1:1 synchronization here. In general $k : m$ synchronization can be defined as the following phase-locking:

$$|kx_n - my_n| < \text{const}$$

for all integers n. For stable periodic orbits of the map (2) the following phase difference is

bounded:

$$|x_n - y_n| < \text{const}$$

and, for the corresponding parameter values, $1:1$ synchronization of the oscillators (1) takes place. Nevertheless one should distinguish between the periodic orbits with zero and nonzero rotation numbers. Only the former correspond to the synchronization in the system, as such trajectories are bounded and they exist inside the Arnol'd tongue for the rotation number zero. Stable periodic orbits that exist inside all other phase-locking regions of nonzero rotation numbers do not lead to a synchronization in the system since such trajectories tend to infinity in the corresponding lift from the circle $[0; 2\pi)$ to $\mathbb{R}^1$.

Figure 2 shows phase-locking regions, the so-called Arnol'd tongues of the following rotation numbers: $\rho = 0, \frac{1}{3}, \frac{1}{2}, \frac{1}{1}$. Figure 3 gives an enlargement with some very narrow tongues. Each tongue emanates from a point $(p/q, 0)$ for integer p and q, and corresponds to the existence of stable and unstable periodic orbits of period q and of the rotation number p/q. Rotation number is a number between 0 and 1 [8], which measures the average amount points are rotated by an iteration of the map. It is defined as follows:

$$\rho = \frac{1}{2\pi} \lim_{n\to\infty} \frac{z_n - z_0}{n},$$

where z_n in (2) is calculated without the $\mod 2\pi$ term.

For the parameter values in between the Arnol'd tongues we have quasiperiodic behaviour, and the phase difference z_n varies in the interval $[0, 2\pi)$ but never returns to its original value, therefore there is no synchronization of the oscillators (1) for these values of the parameters.

For the values of K such that $K < 1$ the map (2) is invertible, the Arnol'd tongues do not intersect, and the system can exhibit only periodic or quasiperiodic dynamics. We are also interested in larger values of K since for $K > 1$ significant regions of the phase synchronization can be found. Moreover, for these parameters values some interesting phenomena which do not occur for the invertible as well as time-continuous systems can be observed.

The widest phase-locking region for the rotation number $\rho = 0$ is bounded by the line $K = 2\pi(\nu_1 - \nu_2)$ which is a saddle-node bifurcation line for the stable and unstable fixed points existing inside the tongue. It is the lower desynchronization line in Fig. 2, and for the parameter values such that $K < 2\pi(\nu_1 - \nu_2)$ no fixed point exists.

Beyond the line $K = 1$ the map (2) becomes noninvertible. With an increase in K inside the tongue, a period-doubling cascade occurs until the dynamics become chaotic and the synchronization is lost at the upper desynchronization line.

The graphs of the sine circle map (2) in Fig. 4 can explain different types of the system behaviour in more details. Fig. 4 (*a*) shows the simplest situation, when all the trajectories are attracted to the stable fixed point. The first boundary crisis line *BC1* in Fig. 2 corresponds to the graph in Fig. 4 (*b*), when the maximum value of the map becomes equal to the value of the unstable fixed point $z^{(u)} + 2\pi$. The second boundary crisis line *BC2* represents the analogous situation but for the minimum value which becomes equal to $z^{(u)} - 2\pi$. Fig. 4 (*d*) shows the graph of the map at the point where these two lines cross. The line *BC3* corresponds to the situation

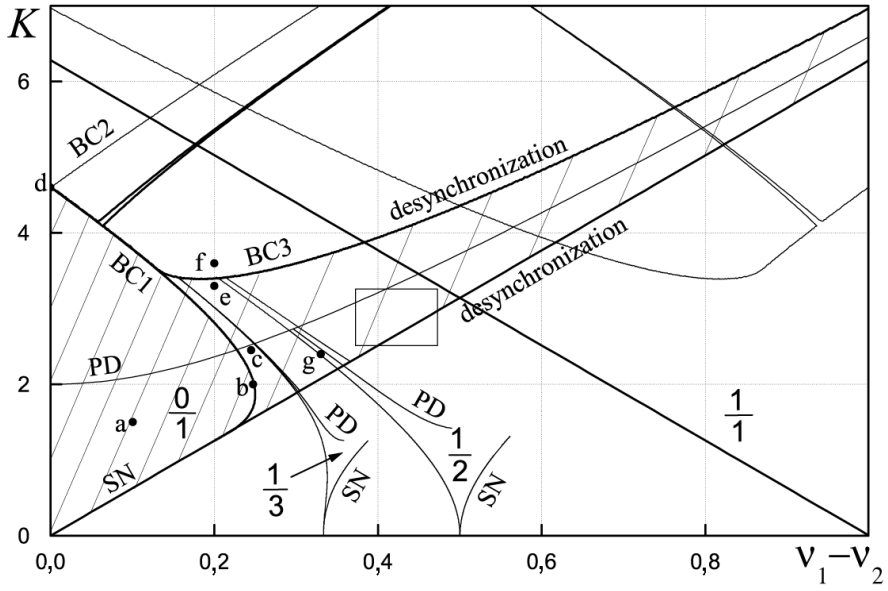

Fig. 2. Region of the phase synchronization of the system (1) and bifurcation curves for the sine circle map (2): SN saddle-node, PD period-doubling, BC boundary crisis; the fractions show the rotation numbers for the corresponding Arnol'd tongues; the region of the rectangle is enlarged in Fig. 3; the points $a-g$ show the parameter values for the graphs of the map (2) in Figs. 4 and 5.

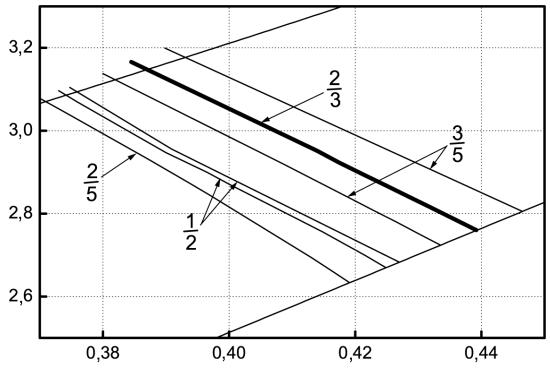

Fig. 3. Enlargement of the rectangle from Fig. 2.

when the minimum value reaches the values of the channel appearing after the first boundary crisis (see Fig. 4 (*f*)). Then, the trajectories come to the unstable fixed point $z^{(u)} + 2\pi$ after the second iteration.

As shown in Fig. 4 (*c*) after the first crisis *BC1*, depending on initial conditions a trajectory of the map (2) can be immediately attracted to the stable fixed point $z^{(s)}$, or it can make one or more revolutions around the circle and eventually be attracted by $z^{(s)}$. Both these possibilities

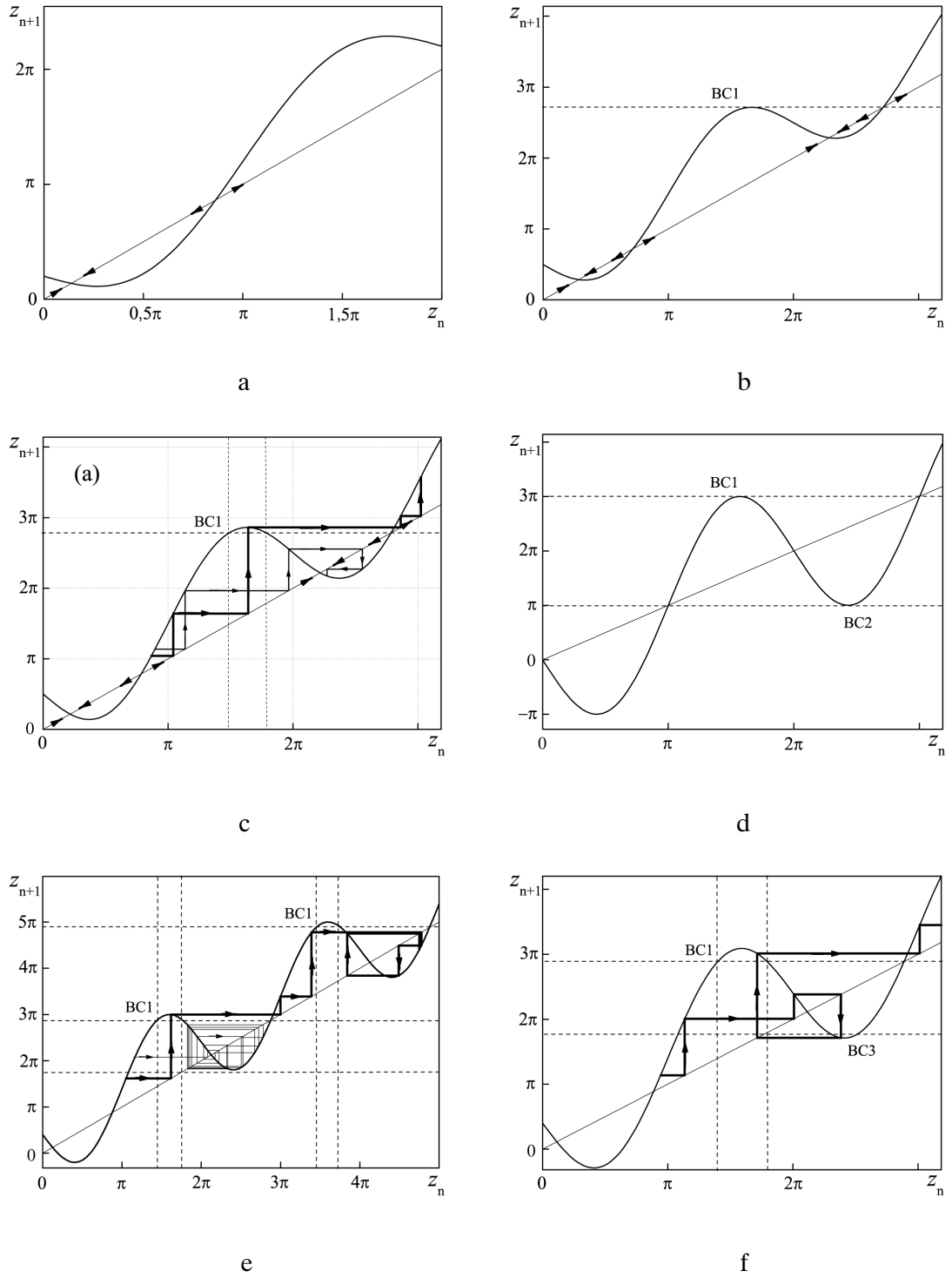

Fig. 4. Appearance of the desynchronous orbits in the map (2); the parameter values for the graphs of the map correspond to the points *a* – *f* from Fig. 2.

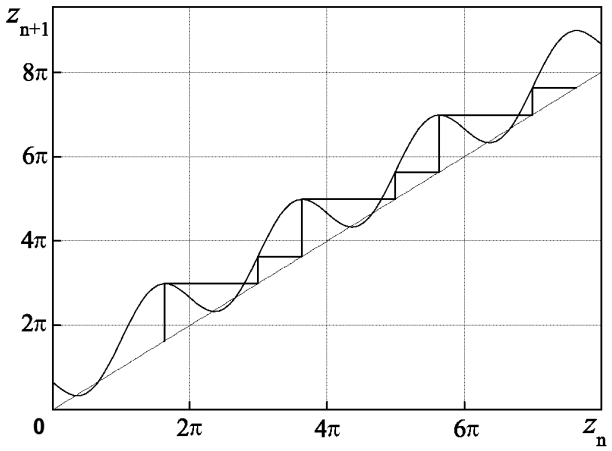

Fig. 5. The superstable period-2 orbit of the map (2) with the parameter values at the point g from the Fig. 2: $\nu_1 - \nu_2 = 0,33$, $K = 2,4$; the rotation number $\rho = 1/2$.

lead clearly to zero rotation number for the trajectory examined. Furthermore the trajectory can make infinitely many rotations, i. e., tend to infinity in the corresponding lift from the circle $[0; 2\pi)$ to $\mathbb{R}^1$. This behaviour can lead to a nonzero rotation number and, hence, desynchronization. As an example, in Fig. 5 we showed the superstable trajectory with rotation number $\rho = \dfrac{1}{2}$, which is a period-2 orbit, attracting all the trajectories that are not attracted to any of the fixed points. Therefore for the same parameter values beyond *BC1*-crisis one can observe trajectories with different rotation numbers depending on the original point from which a trajectory is calculated. Such a situation means a coexistence of synchronization and desynchronization.

Finally, after the boundary crisis *BC3*, almost all trajectories do not exhibit zero rotation numbers, and consequently, there is no synchronization for these parameter values. Fig. 4 (*e, f*) show trajectories and the graphs of (2) before and after the crisis *BC3*, correspondingly. Before the crisis the fixed point has already lost its stability but there exist other attracting states as well as desynchronized trajectories which have arisen after the first *BC1* crisis. But after the *BC3* crisis no more synchronized orbits exist and almost all trajectories tend to infinity.

Figure 6 shows that for many different pairs of K and $\nu_1 - \nu_2$ one can observe at least two different rotation numbers if the trajectories are calculated from different initial conditions. To obtain this figure, for every pair of the parameter values we considered about 300 initial conditions uniformly distributed in the interval $[0, 2\pi)$ and obtained either zero or some particular nonzero rotation number. Figures 2 and 3 show several of the widest and most well defined regions of such a coexistence where two different Arnol'd tongues intersect.

For small values of the difference $\nu_1 - \nu_2$ the first boundary crisis line coincides with the upper desynchronization line, the line beyond which almost all trajectories do not exhibit zero rotation numbers (see Fig. 2). In general for the values of K beyond this line one can find different multistability regions as well as some trajectories with rotation number zero. To illustrate the loss of the synchronization with increasing K, in Fig. 7 we plotted the rotation numbers ρ of the trajectories for different nonlinearities K while $\nu_1 - \nu_2$ were fixed with the values 0,005,

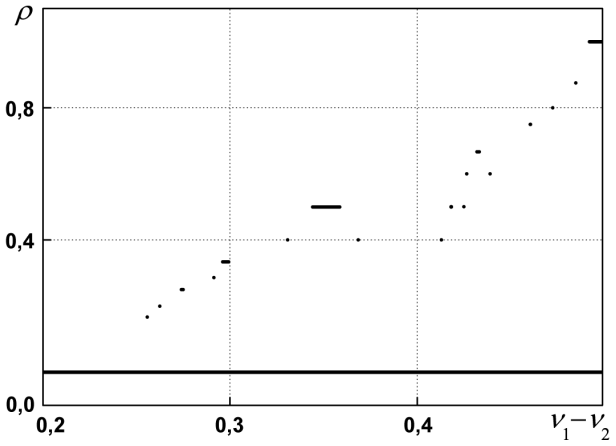

Fig. 6. Rotation numbers of the trajectories of the map (2) starting from different initial conditions. The values of $\nu_1 - \nu_2$ and K are changed inside the Arnol'd tongue for $\rho = 0$, along the right boundary.

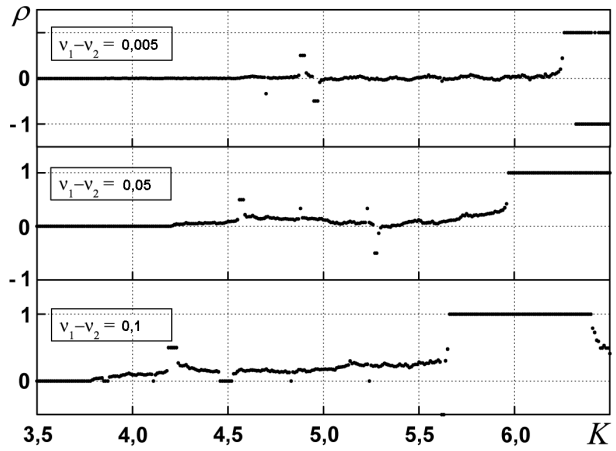

Fig. 7. Rotation numbers ρ for the trajectories of the map (2).

0,05 and 0,1. For every pair of the parameter values $(\nu_1 - \nu_2, K)$ we calculated ρ for trajectories with about 300 different initial conditions. As shown in Fig. 7 for these parameter values multistability is not typical as there are almost no intersections of the Arnol'd tongues. One can see that for smaller values of $\nu_1 - \nu_2$ after desynchronization the rotation numbers change from zero to very small positive or negative values and a number of synchronized states can also be observed. With an increase in the difference of frequencies, the rotation numbers become nonzero more abruptly and take larger values. Figure 8 shows an overview of the parameter region beyond our desynchronization line for which one can observe the trajectories with rotation number smaller than 0,001 in absolute value.

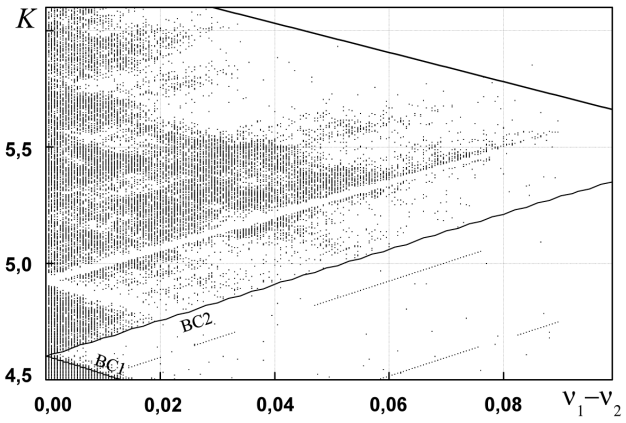

Fig. 8. Black points denote the values of the parameters for which a trajectory exists with rotation number smaller than 0,001 in absolute value.

3. Dynamics of the three-dimensional system. Now let us continue our analysis for the following system of three globally coupled phase oscillators:

$$\begin{aligned} x_{n+1} &= x_n + 2\pi\nu_1 + \frac{K}{3}\big[\sin(y_n - x_n) + \sin(z_n - x_n)\big], \\ y_{n+1} &= y_n + 2\pi\nu_2 + \frac{K}{3}\big[\sin(x_n - y_n) + \sin(z_n - y_n)\big], \\ z_{n+1} &= z_n + 2\pi\nu_3 + \frac{K}{3}\big[\sin(x_n - z_n) + \sin(y_n - z_n)\big], \end{aligned} \tag{6}$$

where the phase variables are calculated modulo 2π. After successive subtracting the second and the third equations from the first one, our system can be reduced to the following two-dimensional system:

$$\begin{aligned} u_{n+1} &= u_n + 2\pi\Delta_1 + \frac{K}{3}\big[-2\sin u_n + \sin v_n - \sin(u_n + v_n)\big], \\ v_{n+1} &= v_n + 2\pi\Delta_2 + \frac{K}{3}\big[-2\sin v_n + \sin u_n - \sin(u_n + v_n)\big], \end{aligned} \tag{7}$$

where $u_n = x_n - y_n$, $v_n = z_n - x_n$, $\Delta_1 = \nu_1 - \nu_2$, $\Delta_2 = \nu_3 - \nu_1$.

Let us consider different cases of the system (7).

3.1. Symmetric case $\Delta_1 = \Delta_2 = 0$**.** This is the case of three identical phase oscillators, i. e., their frequencies are equal, $\nu_1 = \nu_2 = \nu_3$. The system (7) has the following six fixed points with corresponding eigenvalues:

$O(0,0)$, $\lambda_1 = \lambda_2 = 1 - K$, which is an attracting node for $K < 2$,

$S_1(\pi,0)$, $S_2(\pi,\pi)$, $S_3(0,\pi)$, $\lambda_1 = 1 - \dfrac{K}{3}$, $\lambda_2 = 1 + K$, saddles with $|\lambda_1| < 1$ for $K < 6$ and $\lambda_2 > 1$ for all positive K,

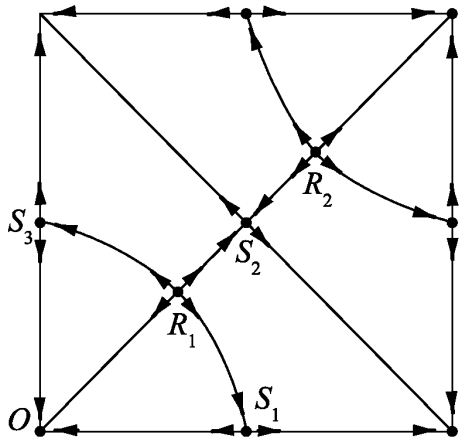

Fig. 9. Phase portrait of the system (7) with $\Delta_1 = \Delta_2 = 0$.

$R_1\Big(\frac{2\pi}{3}, \frac{2\pi}{3}\Big)$, $R_2\Big(\frac{4\pi}{3}, \frac{4\pi}{3}\Big)$, $\lambda_1 = \lambda_2 = 1 + \frac{K}{2}$, repelling nodes for all positive K.

Phase portrait of the system with $\Delta_1 = \Delta_2 = 0$ is shown in Fig. 9.

3.2. $\Delta_1 = \Delta_2 > 0$**.** Denote $\Delta \stackrel{\text{df}}{=} \Delta_1 = \Delta_2$. Then for the system (7) which is defined on the two-dimensional torus $\mathbb{T}^2 = [0, 2\pi)^2$, the diagonal $D = \big\{(u_n, v_n) \in \mathbb{T}^2 : u_n = v_n\big\}$ is an invariant manifold. This implies that the points from D are again mapped into some points on this line, while for any nonvanishing difference between the values of Δ_1 and Δ_2 the dynamics becomes two dimensional and the diagonal is not invariant anymore.

In the manifold D, system (7) is reduced to the following one-dimensional map:

$$u_{n+1} = u_n + 2\pi\Delta - \frac{K}{3}\big[\sin(u_n) + \sin(2u_n)\big]. \tag{8}$$

The map has two pairs of fixed points O, R_1 and S_2, R_2, which are born in the saddle-node bifurcations at $K \approx 1,7 \cdot 2\pi\Delta$ and $K \approx 8,1 \cdot 2\pi\Delta$. Figure 10 shows the corresponding saddle-node bifurcation lines as well as several major Arnol'd tongues. Both stable fixed points O and S_2 lose their stabilities through period-doubling bifurcations. The bifurcation line for O is denoted as PD in Fig. 10 (for S_2 the bifurcation occurs for $K > 6$). As shown in Fig. 10 other Arnol'd tongues cross the widest tongue of the rotation number $\rho = 0$ beyond the boundary crisis line, and this implies coexistence of the trajectories with different rotation numbers, as was described for the sine circle map, see Section 2.3.

As was described above for the sine circle map (2), appearance of the desynchronous orbits can be caused by a boundary crisis, when the maximum or the minimum value of the map becomes equal to the corresponding value of the unstable fixed point. The map (8) is bimodal and has two pairs of the fixed points. Therefore for this map a few additional boundary crises may occur as compared with the map (2). Fig. 11 shows the regions of synchronization and coexistence of synchronous and desynchronous trajectories for the map (8) and Fig. 12 illustrates appearance of the desynchronous trajectories after the crises *BC1 – BC5* as denoted in Fig. 11.

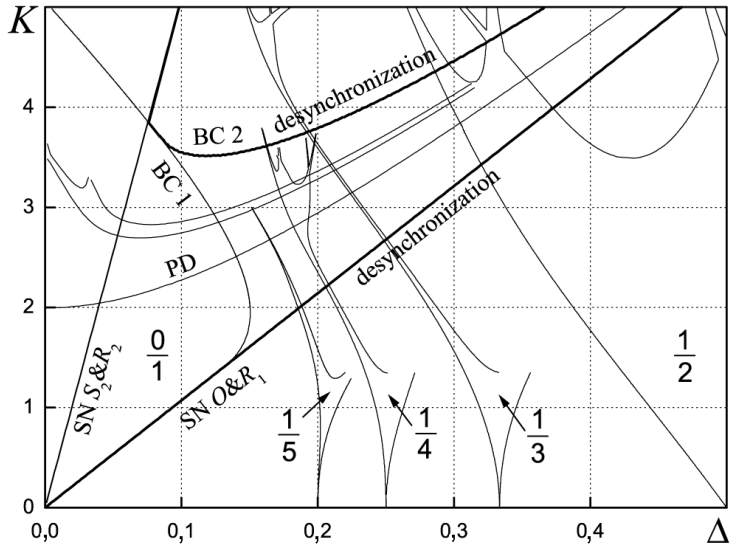

Fig. 10. Arnol'd tongues for the system (6) with $\Delta_1 = \Delta_2 = \Delta > 0$ and $u_n = v_n$; the bifurcation curves for the map (8) are denoted as follows: *SN* $O\&R_1$, *SN* $S_2\&R_2$ the saddle-node bifurcations for the corresponding fixed points, *BC1*, *BC2* are boundary crises.

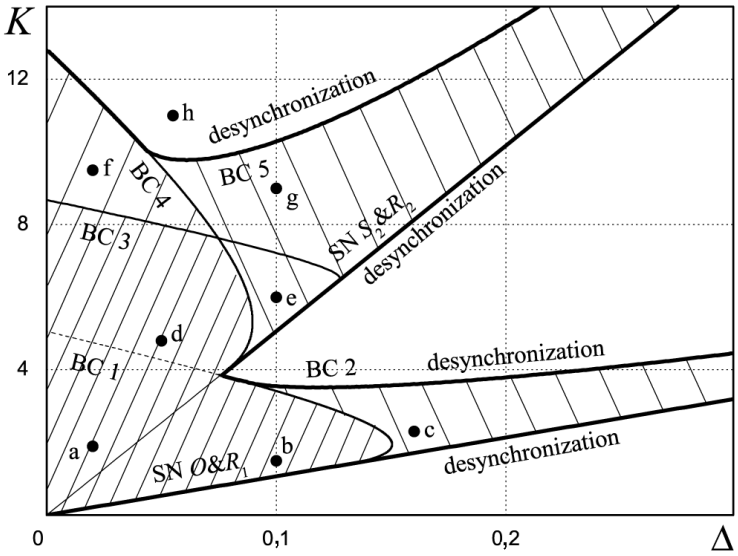

Fig. 11. Regions of the synchronization and coexistence of synchronous and desynchronous trajectories for the map (8), the points $a-h$ correspond to parameter values for the graphs in Fig. 12, *BC1* – *BC5* denote the boundary crisis lines.

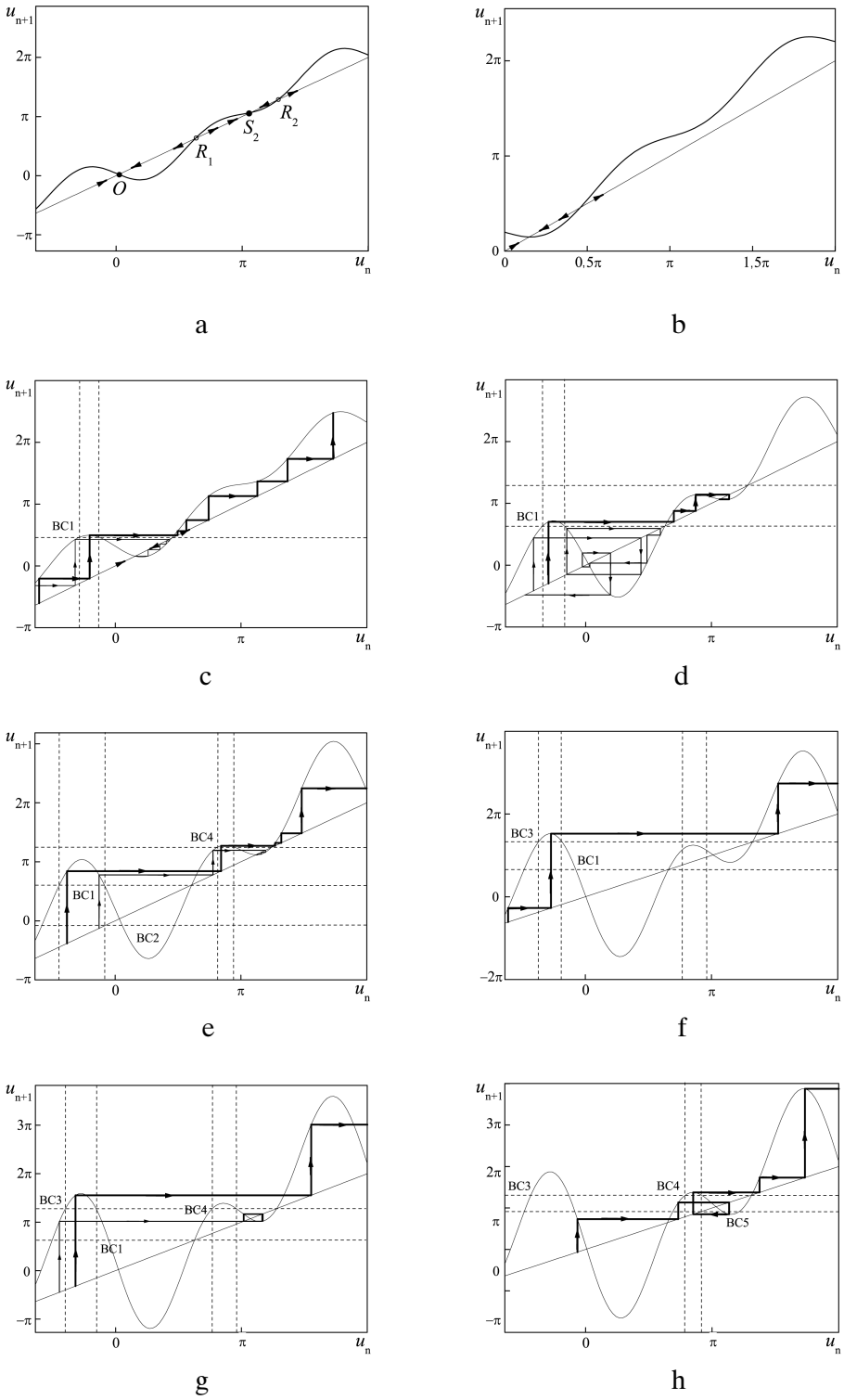

Fig. 12. Appearance of desynchronous orbits for the map (8) with the parameter values at the points $a-h$ from Fig. 11, the designations *BC1 – BC5* correspond to the boundary crises as in Fig. 11.

Coming back to the two-dimensional system (7), first we shall look at the transverse stability of the fixed points O and S_2 or, more generally, the transverse stability of the invariant manifold D. For any point on the diagonal, the system (7) has two eigendirections: $(1, 1)$ along the diagonal and $(1, -1)$ perpendicular to it. The eigenvalue that corresponds to the transversal direction is $1 - K\cos u_n$ and for any orbit $\{u\}_{n=1}^{\infty}$ in the diagonal D the transversal Lyapunov exponent $\lambda_\perp$ is equal to

$$\lambda_\perp = \lim_{N\to\infty} \frac{1}{N} \sum_{n=1}^{N} \ln|1 - K\cos u_n| .$$

The transversal Lyapunov exponent $\lambda_\perp$ gives an insight into stability of the periodic orbits or chaotic one-dimensional attractors in the plane. If $\lambda_\perp$ for an attractor existing on the diagonal is negative then this attractor attracts almost all trajectories from its two-dimensional neighborhood. In Fig. 10 we outlined the parameters regions for which the fixed points and some periodic orbits attract trajectories from the diagonal D, and in Fig. 13 the curves with hachures separate regions where the transversal Lyapunov exponents of the corresponding attractors are negative (area with hachures) and positive (the other side). Thus the fixed point O and the higher-periodic orbits existing in the main Arnol'd tongues are transversally stable for smaller values of coupling K, while the periodic orbits born in the period-doubling cascade from the fixed point O remain transversally stable for larger K but lose their stability with an increase in Δ. In Fig. 14 we plotted the graphs of $\lambda_\perp$ of the points O and S_2 as functions of K for $\Delta = 0,001$. They show that the fixed point S_2 is always transversally unstable, while O loses its transverse stability after $K = 2$, at the corresponding bifurcation line with hachures which is shown in Fig. 13.

Figure 13 also shows the line of the transverse pitchfork bifurcation denoted an $P\,S_1\&R_1\&S_3$. In the bifurcation the saddle point R_1 transforms to an unstable node giving rise to two saddles S_1 and S_3. The phase portrait of the system (7) after this bifurcation is shown in Fig. 15.

3.3. $\Delta_1 = 0$, $\Delta_2 \in [0, 1]$. Let us fix the first difference $\Delta_1 = 0$ and consider the parameter plane $(\Delta_2; K)$. In this case the v_n-axis $V_0 = \{(u_n, v_n) \in \mathbb{T}^2 : u_n = 0\}$ is an invariant manifold, and the dynamics in the manifold is governed by the sine circle map (2). Therefore the regions of existence and stability of the fixed point and other periodic orbits inside the manifold coincide with the Arnol'd tongues of the one-dimensional sine circle map (2), some of these regions are shown in Fig. 16. Apart from the manifold, other attractors exist outside the v_n-axis. As shown in Fig. 9, in the case $\Delta_1 = \Delta_2 = 0$, there exist 6 fixed points. Four of them, S_1, S_2, R_1 and R_2, are located outside the manifold V_0. We find that with increasing Δ_2 they disappear simultaneously through the saddle-node bifurcations at $K \approx 4\cdot 2\pi\Delta_2$. The corresponding phase portraits before and after the bifurcations are shown in Fig. 17. With further increase in Δ_2 the fixed points O and S_3 collide and disappear in the saddle-node bifurcation at $K = 2\pi\Delta_2$, and this implies desynchronization of the system.

With an increase in the coupling K, the stable fixed point O loses its transverse stability through a period-doubling bifurcation (*PD1* curve in Fig. 16) and the stability in V_0 through the bifurcation *PD2*. With more increase in K, the period-2 orbit which was born in the bifurcation *PD1* undergoes a Naimark – Sacker bifurcation (*NS* curve in Fig. 16), while after the bifurcation *PD2*, which takes place in the manifold V_0, a period-doubling cascade occurs. All the points of the periodic orbits of this cascade have $u_n = 0$ and therefore remain on the v_n-axis.

3.4. General case $\Delta_1 \neq \Delta_2$**.** Let us consider several nonzero values of Δ_1 in the system (7) and investigate how the shape of the phase-locking tongues in the plane $(\Delta_2; K)$ changes

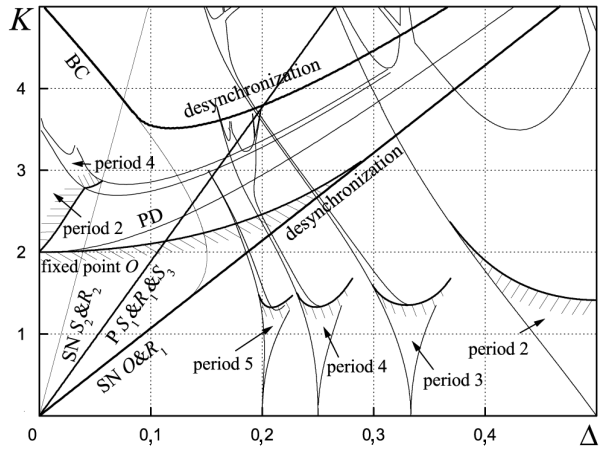

Fig. 13. Regions of the transverse stability of several higher-periodic orbits, the curves with hachures denote the boundaries of the regions where the transversal Lyapunov exponents of the corresponding attractors are negative; $P\ S_1\&R_1\&S_3$ is the transverse pitchfork bifurcation.

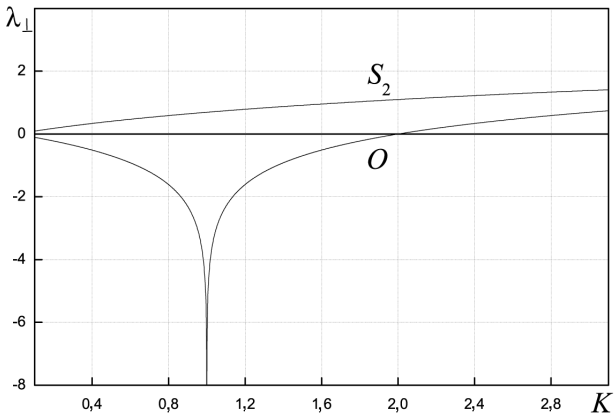

Fig. 14. Variation of the transversal Lyapunov exponents of the fixed points O and S_2 with the coupling parameter K for $\Delta = 0,001$ in the map (8).

for different fixed values of Δ_1. Figure 18 shows several major Arnol'd tongues for $\Delta_1 = 0,1$. One can see that their symmetry with respect to the line $\Delta_2 = 0,5$ is lost, as we have the interaction of two nontrivial frequencies in the system. Moreover the synchronization regions do not emerge from the points on the Δ_2-axis and do not have the exact shape of the tongues any more. This means that for small values of $K \leq 0,5$ the system (6) cannot be synchronized. With further increase in Δ_1 the synchronization regions move away from the Δ_2-axis and become smaller, since for larger Δ_1 it becomes more difficult for the system to achieve the synchronization.

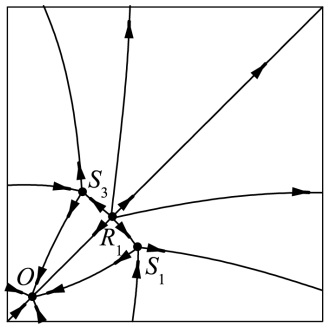

Fig. 15. Phase portrait of the system (7) with the values of Δ and K after the pitchfork bifurcation $S_1\&R_1\&S_3$ has occurred.

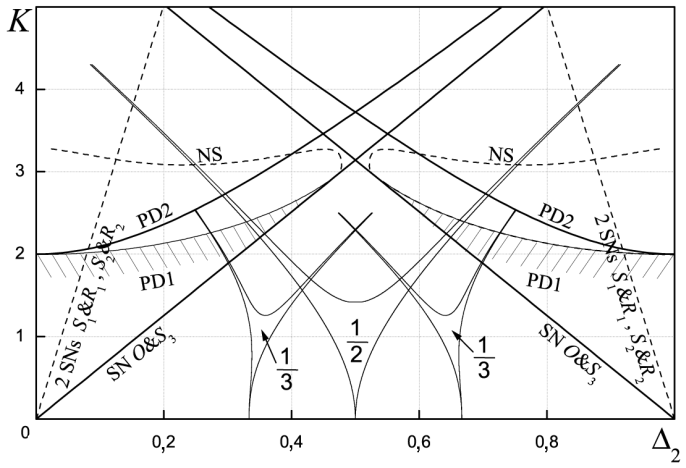

Fig. 16. Arnol'd tongues for the system (6) when the difference $\Delta_1 = 0$. The dashed lines correspond to the bifurcations of the attractors existing or emerging outside the manifold V_0; the bifurcation lines are denoted as follows: *SN* saddle-node, *2* SN_s two simultaneous saddle-node bications, *PD1* transverse period-doubling, *PD2* period-doubling in the manifold V_0, *NS* Naimark – Sacker bifurcations for the period-2 orbit born in the transverse period-doubling bifurcation.

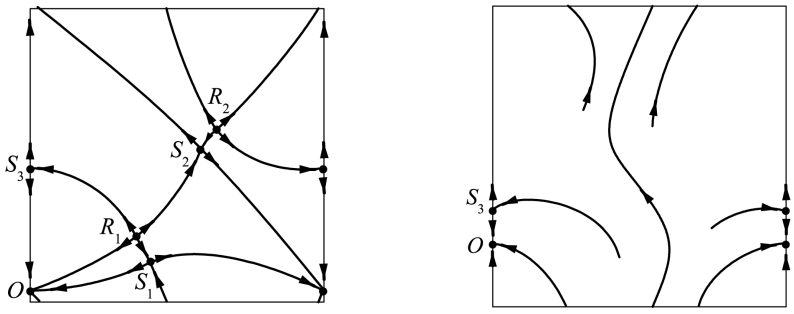

Fig. 17. Phase portraits of the system (7) with $\Delta_1 = 0$ before and after the saddle-node bifurcations $S_1\&R_1$ and $S_2\&R_2$.

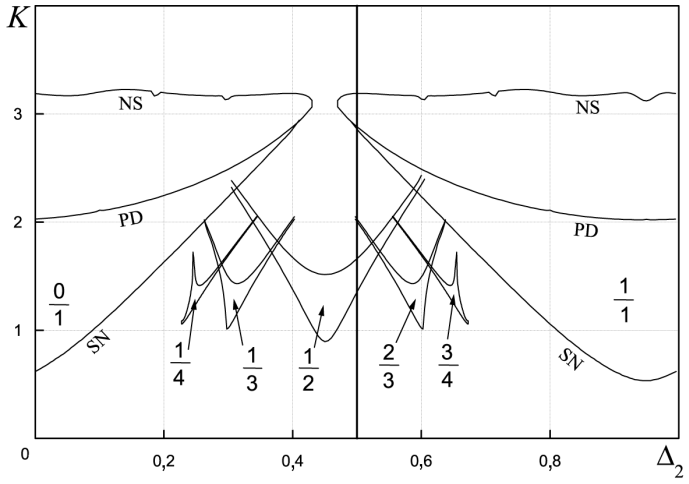

Fig. 18. Regions of stability of higher-periodic orbits of the system (6) when $\Delta_1 = 0, 1$. The bifurcation lines: *SN* saddle-node, *PD* the first period-doubling, *NS* the Naimark – Sacker bifurcation for the period-2 orbit born in the transverse period-doubling bifurcations.

4. Conclusions. In this paper we considered the dynamics of two- and three-dimensional systems of globally coupled shift circle maps with sine-coupling. To investigate the phase synchronization in the systems we considered the corresponding maps for the differences of our original phase variables and studied stability and bifurcations of the equilibria. We also compared the discrete-time model with the continuous-time Kuramoto system and concluded that in the case of the difference equations the system exhibits many more equilibria and dynamical phenomena which cannot be observed for the Kuramoto system.

In the case $N = 2$ the dynamics of the difference $x_n - y_n$ are described by the well-known Arnol'd sine circle map. We plotted several Arnol'd tongues for the higher-periodic orbits and explained how the loss of synchronization occurs with varying the parameters. We also emphasized that for values of the coupling constant K larger than 1, when Arnol'd map is noninvertible, for the same parameter values one can observe trajectories with different rotation numbers in the regions of intersection of different Arnol'd tongues, and hence coexistence of synchronous and desynchronous orbits. We described in detail the boundary crises and bifurcations occurring in our system.

When $N = 3$ the system for the differences $x_n - y_n$ and $z_n - x_n$ is two-dimensional and more complicated than the single equation in the case $N = 2$. Therefore for the system of three coupled oscillators we considered several particular cases. In the case when all three oscillators have the same frequencies we found the exact coordinates of the fixed points and plotted the phase portrait of the system. Then we considered the case when the frequencies of two of our oscillators differ from the frequency of the third one by some quantities that are opposite in sign but equal in absolute value. Under such a condition the problem can be reduced to the one-dimensional equation for the difference $x_n - y_n$. This map describes the dynamics on the diagonal which is an invariant manifold in the case. We explained the trajectories behaviour in the manifold as well as the transversal stability of the fixed points and higher-periodic orbits of the map. Furthermore we considered a two-dimensional case when the difference between

the frequencies of two of the oscillators is fixed to be zero and the third oscillator differs from the two others. In this case the v_n-axis is an invariant manifold and the dynamics on the manifold are described by the one-dimensional sine circle map. Apart from the attractors on the manifold several other fixed points exist, and we plotted the corresponding phase portraits and described the bifurcations for these equilibria. Finally we considered the general case when all the frequencies of our oscillators are different, and we explained briefly how the phase-locking regions change with changing the differences of the frequencies.

5. Acknowledgements. A. Vasylenko and Yu. Maistrenko are grateful for the hospitality of the Laboratory of Nonlinear Systems, Swiss Federal Institute of Technology. A. Vasylenko acknowledges the scholarship of the Swiss Government.

1. *Mosekilde E., Maistrenko Yu., and Postnov D.* Chaotic synchronization. Application to living systems. — New Jersey: World Sci., 2002. — 428 p.
2. *Mosekilde E.* Topics in nonlinear dynamics. — Singapore: World Sci., 1996. — 380 p.
3. *Pikovsky A., Rosenblum M., and Kurths J.* Synchronization — a universal concept in nonlinear sciences. — Cambridge: Cambridge Univ. Press, 2001. — 496 p.
4. *Kittel A., Parisi J., and Pyragas K.* Generalized synchronization of chaos in electronic circuit experiments // Physica D. — 1998. — **112**. — P. 459 – 471.
5. *Blekhman I.* Synchronization in science and technology. — New York: Asme Press, 1988.
6. *Kuramoto Y.* Chemical oscillations, waves and turbulence. — Berlin: Springer, 1984.
7. *Maistrenko Yu., Popovych O., Burylko O., and Tass P.* Mechanism of desynchronization in the finite-dimensional Kuramoto model // Phys. Rev. Lett. — 2004. — **94**, №8.
8. *Devaney R.* An introduction to chaotic dynamical systems. — Redwood City: Addison-Wesley, 1989. — 336 p.

Received 27.04.2004